



1

2 **The Impacts of Biomass Burning Activities on Convective Systems in**  
3 **the Maritime Continent**

4

5 Hsiang-He Lee<sup>1\*@</sup> and Chien Wang<sup>1,2\*\*</sup>

6

7 <sup>1</sup> Center for Environmental Sensing and Modeling, Singapore-MIT Alliance for Research  
8 and Technology, Singapore

9 <sup>2</sup> Center for Global Change Science, Massachusetts Institute of Technology, Cambridge,  
10 MA, U.S.A.

11 \*Now at Atmospheric, Earth, and Energy Division, Lawrence Livermore National  
12 Laboratory, Livermore, CA, U.S.A.

13 \*\*Now at Laboratoire d'Aerologie/CNRS/University of Toulouse, Toulouse, France

14

15

16

17

18

19

20

21

22

23

24

25

26

27

28

29

30

31 @Corresponding author address: Dr. Hsiang-He Lee, 7000 East Avenue, Livermore, CA,  
32 94550, U.S.A.

33 E-mail: lee.hsianghe@gmail.com



## 34 **Abstract**

35        Convective precipitation associated with Sumatra squall lines and diurnal rainfall  
36 over Borneo is an important weather feature of Maritime Continent in Southeast Asia.  
37 Over the past few decades, biomass burning activities have been widespread during  
38 summertime over this region, producing massive fire aerosols. These additional aerosols  
39 brought to the atmosphere, besides influencing local radiation budget through directly  
40 scattering and absorbing sunlight, can also act as cloud condensation nuclei or ice nuclei  
41 to alter convective clouds and precipitation in the Maritime Continent via the so-called  
42 aerosol indirect effects. Based on four-month simulations with or without biomass  
43 burning aerosols conducted using the Weather Research and Forecasting model with  
44 chemistry package (WRF-Chem), we have investigated the aerosol-cloud interactions  
45 associated with the biomass burning aerosols in the Maritime Continent. Results from  
46 selected cases of convective events have shown significant impacts of fire aerosols on the  
47 weak convections in hydrometeors and rainfall amount either in the Sumatra or Borneo  
48 region. Statistical analysis over the fire season also suggests that fire aerosols have  
49 substantial impacts on the nocturnal convections associated with the local anticyclonic  
50 circulation in the western Borneo. In addition, near surface heating from absorbing  
51 aerosols emitted from fires could weaken land breezes and thus the convergence of  
52 anticyclonic circulation. Therefore, the rainfall intensity of the nocturnal convections has  
53 been significantly decreased during the fire events.

54

55



## 56 **1 Introduction**

57 Biomass burning in Southeast Asia has become a serious environmental and societal  
58 issue in the past decade due to its impact on local economy, air quality, and public health  
59 (Miettinen et al., 2011; Kunii et al., 2002; Frankenberg et al., 2005; Crippa et al., 2016;  
60 Lee et al., 2018). Abundant aerosols emitted from such fires not only cause  
61 environmental issues but also affect regional weather and climate through the direct and  
62 indirect effects of biomass burning aerosols (Grandey et al., 2016; Hodzic and Duvel,  
63 2017; Jeong and Wang, 2010; Ramanathan and Carmichael, 2008; Taylor, 2010; Tosca et  
64 al., 2013). Carbonaceous compounds such as black carbon (BC) in biomass burning  
65 aerosols can reduce sunlight through both absorption and scattering to warm the  
66 atmosphere while cool the Earth's surface (Fujii et al., 2014; Andreae and Gelencsér,  
67 2006; Satheesh and Ramanathan, 2000; Ramanathan et al., 2001). Besides these direct  
68 effects, biomass burning aerosols can act as cloud condensation nuclei or ice nuclei to  
69 alter cloud microphysical structures and thus cloud radiation. Such “indirect effects” of  
70 these aerosols on the climate are even more complicated due to various cloud and  
71 meteorological conditions (Sekiguchi et al., 2003; Lin et al., 2013; Wu et al., 2013;  
72 Grandey et al., 2016; Ramanathan et al., 2001; Wang, 2004).

73 For the Maritime Continent in Southeast Asia, convective precipitation associated  
74 with the so-called Sumatra squall lines (SSL) and diurnal rainfall over Borneo is an  
75 important weather feature (Lo and Orton, 2016; Ichikawa and Yasunari, 2006; Koh and  
76 Teo, 2009; Yi and Lim, 2006; Wu et al., 2009). Convections of SSL are initially formed  
77 in the northwestern side of Sumatra by the prevailing sea breezes from Indian Ocean and  
78 the Sumatran mountain range, then propagate over the Malacca Strait affecting the Malay



79 Peninsula. Lo and Orton (2016) analyzed 22-year (1988 to 2009) ground-based Doppler  
80 radar data and identified a total of 1337 squall lines in Singapore. They found that these  
81 events with the diurnal cycle of rainfall most occur during either the summer monsoon  
82 season (June-September) or the inter-monsoon periods (April-May and October-  
83 November). Singapore, for example, experiences typically about 6~7 squall lines per  
84 month during these periods. Oki and Musiaka (1994) analyzed the seasonal and diurnal  
85 cycles of precipitation using rain gauge data and showed that large-scale low-level winds  
86 are a critical modulating factor in the diurnal cycle the convective rainfall over Borneo  
87 besides the general reason of land-sea contrast behind convective rainfall in the Maritime  
88 Continent. Furthermore, Ichikawa and Yasunari (2006) used five years Tropical Rainfall  
89 Measuring Mission (TRMM) precipitation radar (PR) data to investigate the role of the  
90 low-level prevailing wind in modulating the diurnal cycle of rainfall over Borneo. They  
91 found that the diurnal cycle is associated with intraseasonal variability in the large-scale  
92 circulation pattern, with regimes associated with either low-level easterlies or westerlies  
93 over the island.

94 Interestingly, frequent biomass burning activities coincide with vigorous convective  
95 systems in the Maritime Continent, especially during the summer monsoon season (June-  
96 September), and could thus produce aerosols to affect convections in the region.  
97 Rosenfeld (1999) analyzed TRMM data and hypothesized that abundant biomass burning  
98 aerosols could practically shut off warm rain processes in tropical convective clouds.  
99 Compared to the adjacent tropical clouds in the cleaner air, clouds encountered with  
100 smokes could grow to higher altitudes with rain suppressed, hypothetically due to the  
101 reduction of coalescence efficiency of smaller cloud drops into raindrops. Recently,



102 using Weather Research and Forecasting model with Chemistry (WRF-Chem), Ge et al.  
103 (2014) have studied the direct and semi-direct radiative effects of biomass burning  
104 aerosols over the Maritime Continent and found the radiative effect of biomass burning  
105 aerosols could alter planetary boundary layer (PBL) height, local winds (including sea  
106 breeze), and cloud cover. However, relative coarse resolution (27 km) adopted in their  
107 simulation would not be able to reveal more details about how biomass burning aerosols  
108 affect convective clouds through modifying cloud microphysics processes. Whereas,  
109 Hodzic and Duvel (2017) have conducted a 40-day simulation using WRF-Chem with a  
110 convection-permitting scale (4 km) to study the fire aerosol-convection interaction during  
111 boreal summer in 2009 near the central Borneo mountainous region. Their result  
112 suggests that modifications of the cloud microphysics by biomass burning aerosols could  
113 reduce shallow precipitation in the afternoon and lead to a warm PBL anomaly at sunset,  
114 all lead to an enforcement of deep convection at night. However, they have also  
115 indicated that the radiative processes of moderately absorbing aerosols tend to reduce  
116 deep convection over most regions due to local surface cooling and atmosphere warming  
117 that increase the static stability, hence suggesting the complexity of the interaction of  
118 biomass burning aerosols and convective clouds in the Maritime Continent.

119 In this study, we aim to examine and quantify the impacts of biomass burning  
120 aerosols on convective systems over two targeted regions for analyses: the northern  
121 Sumatra and the western Borneo in the Maritime Continent. Our focus is on not only the  
122 change of hydrometeors in the convective clouds but also the change of rainfall amount  
123 and intensity in these regions. We firstly describe methodologies adopted in the study,  
124 followed by the results and findings from our numerical simulations over the Maritime



125 Continent. We have selected three cases in each study region to perform detail analyses.  
126 In addition, statistical analyses covering the entire modeled fire season for each of these  
127 two regions have also been performed to provide more generalized pictures about the  
128 effects of fire aerosol on convection. The last section summarizes and concludes our  
129 work.

## 130 **2 Methodology**

### 131 **2.1 Model and emission inventories**

132 In order to simulate trace gases and particulates interactively with the meteorological  
133 fields, the Weather Research and Forecasting model coupled with a chemistry module  
134 (WRF-Chem, see Grell et al. (2005)) version 3.6.1 is used in this study. Within WRF-  
135 Chem, the Regional Acid Deposition Model, version 2 (RADM2) photochemical  
136 mechanism (Stockwell et al., 1997) coupled with the Modal Aerosol Dynamics Model for  
137 Europe (MADE) as well as the Secondary Organic Aerosol Model (SORGAM)  
138 (Ackermann et al., 1998; Schell et al., 2001) are included to simulate atmospheric  
139 chemistry and anthropogenic aerosol evolutions. MADE/SORGAM uses a modal  
140 approach to represent the aerosol size distribution and predicts mass and number  
141 concentrations of three aerosol modes (Aiken, accumulation, and coarse).

142 To resolve the convective system in the Maritime Continent in our simulations, two  
143 model domains with two-way nesting are designed. Here, Domain 1 ( $431 \times 141$  grid  
144 cells) has a resolution of 25 km, while Domain 2 ( $561 \times 591$  grid cells) has a resolution  
145 of 5 km (Fig. 1). Specifically, Domain 1 is positioned to include the tropical Indian  
146 Ocean on its west half in order to capture the path of Madden-Julian Oscillation (MJO),



147 and in the meantime to have a northern boundary constrained within 23°N in latitude to  
148 avoid potential numerical instability from the terrain of Tibetan Plateau. Domain 2 with  
149 a finer resolution is positioned to cover the mainland Southeast Asia as well as the islands  
150 of Sumatra and Borneo. The National Center for Environment Prediction FiNaL (NCEP-  
151 FNL) reanalysis data (National Centers for Environmental Prediction, 2000) are used to  
152 provide initial and boundary meteorological conditions, and to perform four-dimensional  
153 data assimilation (FDDA) to nudge model temperature, water vapor, and zonal and  
154 meridional wind speeds above the planetary boundary layer (PBL) for Domain 1. The  
155 Mellor-Yamada-Nakanishi-Niino level 2.5 (MYNN) (Nakanishi and Niino, 2009) is  
156 chosen as the scheme for planetary boundary layer in this study. Other physics schemes  
157 adopted in the simulations include Morrison two-moment microphysics scheme  
158 (Morrison et al., 2009), RRTMG longwave and shortwave radiation schemes (Mlawer et  
159 al., 1997; Iacono et al., 2008), Unified Noah land-surface scheme (Tewari et al., 2004),  
160 and Grell-Freitas ensemble cumulus scheme (Grell and Freitas, 2014) (for Domain 1  
161 only).

162 WRF-Chem needs emissions for gaseous and particulate precursors to drive its  
163 simulations. For this purpose, we have used the Regional Emission inventory in ASia  
164 (REAS) version 2.1 (Kurokawa et al., 2013). REAS includes emissions of most primary  
165 air pollutants and greenhouse gases, covering each month from 2000 to 2008. In  
166 addition, the Fire INventory from U.S. National Center for Atmospheric Research  
167 (NCAR) version 1.5 (FINNv1.5) (Wiedinmyer et al., 2011) is also used in the study to  
168 provide biomass burning emissions. FINNv1.5 classifies burnings of extratropical forest,  
169 tropical forest (including peatland), savanna, and grassland. Fire heat fluxes for four



170 different types of fire are prescribed in WRF-Chem to calculate the plume height (rf.  
171 Table 1 in Freitas et al. (2007). For peatland fire, we have set its heat flux as  $4.4 \text{ kW m}^{-2}$ ,  
172 which is the same as that of savanna burning and differs from that of the tropical forest  
173 burning in  $30 \text{ kW m}^{-2}$ . The modified the plume rise algorithm in WRF-Chem to  
174 specifically improve the representation of tropical peat fire has been described in Lee et  
175 al. (2017). It is worth indicating that the heat flux from biomass burning is not  
176 incorporated in thermodynamic equation of current WRF-Chem model.

177 The default chemical profiles of several species in the lateral boundary condition are  
178 higher than their background concentrations in our study region and thus equivalent to  
179 provide additional aerosol sources from boundaries. To prevent this, we have set  $\text{NO}$ ,  
180  $\text{NO}_2$ ,  $\text{SO}_2$ , and all primary aerosol levels to zero at the lateral boundaries of Domain 1.  
181 We have also adjusted the ozone profile used for lateral boundary condition based on the  
182 World Meteorological Organization (WMO) Global Atmosphere Watch (GAW) station  
183 in Bukit Kototabang, Indonesia (Lee et al. (2019).

## 184 **2.2 Numerical experiment design**

185 Two numerical simulations, both include fossil fuel emissions while either with and  
186 without the biomass burning emissions (labeled as FFBB and FF, respectively), have  
187 been conducted to investigate the impacts of biomass burning aerosols on convective  
188 systems in the Maritime Continent through both direct and indirect effects. Our study  
189 focuses on the fire season from June to September of 2008. Therefore, the simulations  
190 start from 1 May of 2008 and last for five months. The first month is used as a spin-up  
191 period. Among the years with available emission data, both emission amount of biomass  
192 burning and total precipitation in 2008 approximate their ensemble mean or represent an



193 average condition. Nevertheless, interannual variation of biomass burning emissions  
194 alongside precipitation in the studies regions do exist (Lee et al., 2017; Lee et al., 2018),  
195 and the influence of such variation on the effects of fire aerosol on convection should be  
196 addressed in future studies.

### 197 **2.3 Analysis methods**

198 The primary target of this study is the convective systems associated with Sumatra  
199 squall lines and diurnal rainfall over Borneo. Thus, our analyses mainly focus on the  
200 convections over two specific regions: the Sumatra region (r1 in Fig. 1) and the Borneo  
201 region (r2 in Fig. 1). The area coverage of the Sumatra region (r1) is from 97° to 103° E  
202 in longitude and 0° to 6° N in latitude, while the area coverage of the Borneo region (r2)  
203 is from 109° to 115° E in longitude and 1° S to 5° N in latitude.

204 To examine the impacts of fire aerosols on cloud formation and rainfall intensity as  
205 well as amount, we have selected three convective systems each for the two focused  
206 regions to perform an in-depth case study. We first trace the path of individual  
207 convections and focus the analyses on the specific area of each of these convective  
208 systems to identify the impacts of fire aerosols. Table 1 shows the selected cases in the  
209 Sumatra region (r1) and the Borneo region (r2).

210 The consequent analyses are then focused on the fire-season-wise statistics of  
211 convections for each study region. Table 2 shows the fire periods in the two study  
212 regions. There are total of 54 convective systems simulated during the fire periods in the  
213 Sumatra region (r1) and 35 convective systems in the Borneo region (r2).



214 The statistical quantities used in this study follows Wang (2005) to estimate the  
215 mean value over a specific region (e.g., r1 or r2). The cloud area mean quantities are  
216 defined as a function of output time step (t) by the following equation:

$$217 \quad \bar{c}^{area}(t) = \frac{1}{N(t)} \sum_{\substack{q > q_{min} \\ n > n_{min}}} c(x, y, z, t). \quad (1)$$

218 Here  $c$  is a given quantity (e.g., cloud water mass). Eq. (1) only applies to the grid points  
219 where both the mass concentration  $q$  and number concentration  $n$  of a hydrometeor  
220 exceed their given minima. The total number of these grid points at a given output time  
221 step  $t$  is represented by  $N(t)$ . The cloud area mean quantities are used to present the  
222 average quantities of a given variable at a given output time step. Note that the cloud  
223 area mean quantities only apply to hydrometeors. For rainfall, the analyzed quantities are  
224 spatial averages over a specific area of the convective system for case study or over the  
225 entire study region for longer-term statistic estimate.

## 226 **3 Results**

### 227 **3.1 Model evaluation**

#### 228 **3.1.1 Precipitation**

229 The satellite-retrieved precipitation of the Tropical Rainfall Measuring Mission  
230 (TRMM) 3B42 3hrly (V7) dataset (Huffman et al., 2007) is used in this study to evaluate  
231 simulated rainfall. Figure 2a and 2b show the Hovmöller plots of daily TRMM and  
232 FFBB precipitation from 1 June 2008 to 30 September 2008, respectively. Compared to  
233 the satellite-retrieved data, the model has captured all the major rainfall events in the two  
234 analysis regions (Fig. 3). In addition, because of its higher spatial resolution than



235 TRMM, the model produces more light rain events. Nevertheless, as indicated in our  
236 previous study (Lee et al., 2017), a wet bias of the model is evident and mainly comes  
237 from water vapor nudging in data assimilation (FDDA). As a result, the daily average  
238 rainfall in FFBB over the Sumatra region (r1) is  $11.05 \pm 5.90$  mm day<sup>-1</sup> from 1 June 2008  
239 to 30 September 2008, higher than that of  $7.21 \pm 5.54$  mm day<sup>-1</sup> derived from TRMM  
240 retrieval. The wet bias also exists in the modeling results in the Borneo region (r2),  
241 where daily average rainfall there is  $15.40 \pm 8.49$  mm day<sup>-1</sup> in FFBB and only  $9.56 \pm 7.20$   
242 mm day<sup>-1</sup> in TRMM. For the simulated rainfall in FFBB, the temporal correlation with  
243 TRMM is 0.44 in the Sumatra region (r1) and 0.64 in the Borneo region (r2).

### 244 **3.1.2 Aerosol optical depth (AOD)**

245 Because of limited ground-based observational data of aerosols, we use Aerosol  
246 Optical Depth (AOD) from the level-3 Moderate Resolution Imaging Spectroradiometer  
247 (MODIS) gridded atmosphere monthly global joint product (MOD08\_M3;  
248 [http://dx.doi.org/10.5067/MODIS/MOD08\\_M3.061](http://dx.doi.org/10.5067/MODIS/MOD08_M3.061)) to evaluate modeled aerosol spatial  
249 distribution and relative concentration. Figure 4a shows MODIS monthly AOD in  
250 Southeast Asia in September 2008. High AOD occurs in the southern part of Sumatra  
251 and the southwestern part of Borneo. Compared to the MODIS retrieval, the modeled  
252 AOD in FFBB has similar spatial distribution but a higher value (Fig. 4b). It is because a  
253 high spatiotemporal resolution in our simulation enables the model to capture episodic  
254 fire events better. In contrast, FF simulation produces much lower AOD values than  
255 those of MODIS and FFBB, thus suggesting biomass burning aerosols make a substantial  
256 fraction in atmospheric AOD during burning seasons.



### 257 **3.1.3 Sounding profiles**

258 We have used multiple weather sounding profiles measured in Bintulu Airport,  
259 Malaysia (113.03° E, 3.20° N), provided by University of Wyoming  
260 (<http://weather.uwyo.edu/upperair/sounding.html>). An example for detailed summary is  
261 a case at 12 UTC on 22 September 2008 (Fig. 5a). This sounding provides information  
262 of atmospheric state (e.g., vertical distributions of pressure, temperature, wind speed,  
263 wind direction, and humidity) coinciding with one of our selected case study (r2c3) of  
264 diurnal convective rainfall in Borneo. Compared to the observed sounding data, the  
265 FFBB simulation has produced similar temperature and wind profiles and well captured  
266 the low-level and high-level wind speeds and wind directions (Fig. 5a versus 5b). It also  
267 well predicts several key indexes of convection: temperature and pressure of the Lifted  
268 Condensation Level (LCL) simulated in FFBB are 296.2 K and 955 hPa, respectively,  
269 which are close to the values of 296.2 K in temperature and 960.7 hPa in pressure derived  
270 from the observed sounding data. The model predicts 3049 J of Convective Available  
271 Potential Energy (CAPE), while 2031 J of CAPE is estimated in the observed sounding  
272 data. Besides this 22 September 2008 case, the model has also captured major features of  
273 observed profiles for all the other cases selected in our analyses.

### 274 **3.1.4 Cloud vertical structure**

275 The Cloud-Aerosol Lidar and Infrared Pathfinder Satellite Observation (CALIPSO)  
276 provides information of the vertical structure of clouds on its path around the globe  
277 ([https://www-calipso.larc.nasa.gov/products/lidar/browse\\_images/production/](https://www-calipso.larc.nasa.gov/products/lidar/browse_images/production/)), including  
278 that of one of our cases (r2c3) of diurnal convective rainfall in Borneo on September 22,



279 2008 (Fig. 6a). For this case, CALIPSO shows the vertical structure of a convective  
280 system over Borneo along with high  $PM_{2.5}$  concentration near the surface (yellowish  
281 color near the surface), implying a potential impact of biomass burning aerosols on  
282 convective clouds. It can be seen that the FFBB simulations well captures the vertical  
283 structure of convective clouds as well as the near-surface aerosol layers, including their  
284 vertical extension (Fig. 6c versus 6a). With the comparison of FF simulation, we are able  
285 to identify the biomass burning origin of these aerosols near the surface.

## 286 **3.2 Analyses of selected cases in two study regions**

### 287 **3.2.1 The Sumatra region (r1)**

288 The three selected cases in r1 or the Sumatra region (r1c1, r1c2 and r1c3) all  
289 occurred in the afternoon (2 PM or 5 PM local time) and lasted less than 24 hours (Table  
290 1). Most fire aerosols in this study region were initially emitted from the central and  
291 south Sumatra then transported along with southwesterly winds to encounter convections  
292 in the northern Sumatra. Compared to the result of FF,  $PM_{2.5}$  concentration in FFBB can  
293 be 6~12 times higher in the Sumatra region (r1) in these selected cases (Fig. 7).

294 Aerosols from biomass burning in FFBB add 2~3 times more cloud droplet number  
295 concentration and 8~20% higher cloud water mass compared to the results in FF (Table  
296 2). The mean radius of cloud droplets in FFBB is about 6~7  $\mu\text{m}$ , clearly smaller than that  
297 in FF (10~11  $\mu\text{m}$ ). Smaller cloud droplet in FFBB reduces the efficiency of  
298 autoconversion, and further decreases rain water mass and raindrop number  
299 concentration. Hence, raindrop number concentration in FFBB is 40~50% lower than  
300 that in FF among our selected cases in r1 (Table 3). However, besides autoconversion,



301 rain water mass is also affected by other microphysics processes. Larger raindrops  
302 combining smaller cloud droplets in FFBB can increase the efficiency of cloud droplet  
303 collection by rain and thus produce higher rain water mass but number, possibly  
304 compensating the decrease of rain water mass resulted from lowered autoconversion.  
305 Overall, rain water mass decreases 15% in the case of r1c2 and 10% in the case of r1c3,  
306 respectively. Compared to the cases of r1c2 and r1c3, the case of r1c1 is a relatively  
307 weak convective system. After introducing fire aerosols, the mass concentration of snow  
308 and graupel in this case increases 62% and 48%, respectively. Melting snow and graupel  
309 in the lower atmosphere results in a significant increase of rain water mass concentration  
310 by 49%. Thus, total hydrometeor mass is increased by 36% in FFBB from that in FF.  
311 Note that the “aerosol-aware” microphysics scheme in WRF-Chem only applies to the  
312 warm cloud process (Morrison et al., 2005; Morrison et al., 2009); therefore, ice  
313 nucleation is parameterized of ambience temperature only regardless of the aerosol  
314 concentration.

315 In the FF simulations, the convective system in the case of r1c2 and r1c3 is stronger  
316 than the system in the case of r1c1, and the average rainfall of r1c2 and r1c3 is also  
317 higher than the rainfall of r1c1 (Table 4). Adding fire aerosols in FFBB does not  
318 substantially change the average rainfall in r1c2 and r1c3 (+3% and -8%, respectively;  
319 Table 4). However, in the relatively weak convective system of r1c1, adding fire  
320 aerosols significantly increases the mean rainfall amount by 106% ( $1.33 \pm 0.47 \text{ mm } 3\text{hr}^{-1}$   
321 in FF versus  $2.74 \pm 1.21 \text{ mm } 3\text{hr}^{-1}$  in FFBB).



### 322 **3.2.2 The Borneo region (r2)**

323 The three selected cases in r2 (r2c1, r2c2, and r2c3) also occurred during the summer  
324 monsoon season when active biomass burning events existed in the west Borneo. In these  
325 cases, fire aerosols were transported to the north and northeast by the southeasterly and  
326 southwesterly winds. Because of the proximity of fire emissions, the  $PM_{2.5}$  concentration  
327 in FFBB can be 24 times higher than that in FF in the Borneo region (r2) in these selected  
328 cases (Fig. 7).

329 The modeled results demonstrate the substantial impacts of fire aerosols on both  
330 ambient aerosol concentration and cloud droplet number concentration.  $PM_{2.5}$   
331 concentration in FFBB is drastically higher than that in FF with the highest increase  
332 appears in the case of r2c1 at 4940%, more than doubled the values of r2c2 (2402%) and  
333 r2c3 (2422%). The increase in cloud droplet number concentration in the case of r2c1  
334 (703%) is also substantially higher than those in r2c2 (337%) and r2c3 (409%) (Table 2).  
335 The mean radius of cloud droplets in FFBB is about 6~7  $\mu m$ , which is substantially  
336 smaller than that in FF (10~11  $\mu m$ ). The mean cloud droplet radii in FF and FFBB in r2  
337 are similar to the results in r1. On the other hand, the increase of cloud water mass due to  
338 fire aerosols is not so dramatic in all these cases, only about 8%~27% higher than that in  
339 the FF simulations (Table 3). As discussed above, rain number concentration in FFBB  
340 over the Borneo region (r2) is lower than that in FF, similar to the cases in r1, likely due  
341 to the low efficiency of autoconversion induced by the presence of a large quantity of  
342 smaller cloud droplets. Rain water mass of FFBB in the r2c1 case is decreased by about  
343 6% due to fire aerosols, which is similar to the results in the r1c2 and r1c3 cases over the  
344 Sumatra region (Table 3). However, interestingly, rain water and snow mass are both



345 substantially increased in FFBB by 64% and 69% in r2c2 and by 19% and 60% in r2c3,  
346 respectively (Table 3). The cases of r2c2 and r2c3 are relatively weak convective  
347 systems, similar to the case of r1c1. Our results show that fire aerosols have substantial  
348 impacts on cold cloud processes in the weak convective systems. Overall, total  
349 hydrometeor mass concentration in FFBB have increased 47% in r2c2 and 13% in r2c3.

350 The changes of rainfall amount due to fire aerosols in r2 are similar to the cases in r1.  
351 For the strong convection case of r2c1, adding fire aerosols in the FFBB simulation  
352 decreases the total rainfall amount by 18%. However, in the weak convection cases of  
353 r2c2 and r2c3, adding fire aerosols would double the rainfall amount (Table 4).  
354 Compared to the results in FF, rainfall intensity is persistently higher in FFBB during the  
355 convection life cycle in those weak convection cases. Nighttime rainfall intensity in  
356 FFBB, especially, is much higher than the rainfall intensity in FF. Therefore, as shown  
357 by our results, fire aerosols appear to have more substantial impacts on the quantities of  
358 hydrometeors and rainfall of the weak convection cases in both Sumatra region (r1) and  
359 Borneo region (r2).

### 360 **3.3 Fire-season statistics of convections in two study regions**

361 Statistics covering the entire simulated fire season (~4 months) for each study region  
362 have been derived to provide trend/tendency information regarding several aspects of the  
363 impact of fire aerosols on convections. In our simulations,  $PM_{2.5}$  concentration in FF  
364 during the fire periods, which can be regarded as the background value for FFBB  
365 simulation before adding fire aerosols, is  $1.36 \pm 0.19 \mu\text{g m}^{-3}$  in r1 and  $0.56 \pm 0.09 \mu\text{g m}^{-3}$  in  
366 r2. In comparison,  $PM_{2.5}$  concentration in FFBB is  $11.37 \pm 10.41 \mu\text{g m}^{-3}$  in r1 and



367  $10.07 \pm 7.73 \mu\text{g m}^{-3}$  in r2. Note that unlike in some other studies where the control  
368 simulations use constant aerosol concentrations, fire aerosol concentrations in our  
369 simulations can vary in responses to changes in fire emissions, or aerosol removal by rain  
370 scavenging due to precipitation change caused by fire aerosols themselves. Hence, the  
371 processes included in our simulations are closer to reality, and the results could better  
372 reflect the nature of fire aerosol-convection interaction in the Maritime Continent.

373 Averaged through the entire modeled fire periods, cloud water mass ( $Q_c$ ), cloud  
374 droplet number concentration ( $Q_{nc}$ ), and rain drop number concentration ( $Q_{nr}$ ) in FFBB  
375 differ substantially from those in FF, demonstrating the influence of fire aerosols. Figure  
376 8 shows that adding fire aerosols in FFBB would increase  $Q_c$  by 14% and  $Q_{nc}$  by 226%  
377 in r1, and  $Q_c$  by 18% and  $Q_{nc}$  by 349% in r2. Another pronounced change in response to  
378 adding fire aerosols is a decrease in  $Q_{nr}$  by 44% in r1 and 47% in r2. Although an  
379 increase in snow mass ( $Q_s$ ) and graupel mass ( $Q_g$ ) and a decrease in rain water mass ( $Q_r$ )  
380 after adding fire aerosols, the uncertainty of these hydrometeor changes is large.

381 In Sect. 3.2, we have discussed the significant rainfall increase occurred in the weak  
382 convective systems after adding fire aerosols. Here we use the fire-season statistics to  
383 further this discussion. Regardless the strength of convective precipitation, the mean 3-  
384 hourly rainfall during the fire periods is  $1.06 \pm 0.85 \text{ mm } 3\text{hrs}^{-1}$  in FF and  $1.09 \pm 0.86 \text{ mm } 3\text{hrs}^{-1}$   
385  $3\text{hrs}^{-1}$  in FFBB over the Sumatra region (r1), statistically does not change. The rainfall  
386 difference in the Borneo region (r2) between FF and FFBB is also insignificant  
387 ( $1.32 \pm 1.20 \text{ mm } 3\text{hrs}^{-1}$  in FF versus  $1.35 \pm 1.14 \text{ mm } 3\text{hrs}^{-1}$  in FFBB).

388 On the other hand, based on the diurnal rainfall pattern in two study regions, we  
389 notice that daily maximum and minimum rainfall show apparent differences between the



390 FFBB and FF simulations in r2, while such differences are rather small in r1 (Fig. 9).  
391 The maximum or minimum rainfall intensity in the two simulations are closely aligned  
392 with the 1:1 line in Fig. 9a and 9b. However, when looking into each of the 54  
393 convective events in r1, there are 30 events where the model predicted higher maximum  
394 and minimum rainfall intensity in FFBB than in FF. These are mostly weak convective  
395 events.

396 Additionally, and somewhat opposite to the rainfall statistics in r1, the intensity of  
397 maximum and minimum rainfall in r2 is higher in FF than in FFBB. The daily rainfall  
398 peak in r1 is mostly less than  $3 \text{ mm } 3\text{hrs}^{-1}$ ; in comparison, one-third of convective events  
399 in r2 have daily maximum rainfall exceeding  $3 \text{ mm } 3\text{hrs}^{-1}$ . We have categorized the  
400 maximum rainfall based on its values in the afternoon and midnight. We find that those  
401 heavy maximum rainfalls in r2 tend to occur in the midnight (Fig. 9c) associated with the  
402 anticyclonic circulation formed in the western Borneo induced by southeasterly winds  
403 from the Southern latitude turn northeastward along the west coast of Borneo, owing to  
404 the terrain of Borneo Island and the sea breezes from the South China Sea. The vortex  
405 produced by such a circulation leads to strong updraft and then strong convection. Note  
406 that this anticyclonic circulation is different from the Borneo vortex, the latter appears as  
407 a persistent feature of the boreal winter climatology and is related to the northeasterly  
408 from the South China Sea and cold surge events (Chang et al., 1983; Chang et al., 2005).

409 The low-level wind pattern of Borneo convections is similar to the westerly regime,  
410 especially the weak westerly (WW) regime identified by Ichikawa and Yasunari (2006).  
411 According to their analysis, the WW regime tends to occur in boreal summer. Its  
412 composites include an anticyclonic feature with the weak wind field over the Borneo



413 Island. The deep convective storms developed in the WW regime tend to stay close to  
414 the west coast associated with the lower-level convergence enhanced by the prevailing  
415 wind and local circulations around there, resulting in localized rainfall over the offshore  
416 region of the west coast. Based on our simulations, the onset of convection occurs in the  
417 afternoon over the western mountain range of Borneo. These storms would consequently  
418 evolve into widespread shallow storms in the evening over the western part of the island.  
419 The maximum rainfall appears on the west coast because of a local westward propagating  
420 rainfall system that develops around midnight or early morning.

421 The comparison of the maximum rainfall between FF and FFBB in Fig. 9 shows that  
422 fire aerosols tend to reduce the maximum rainfall, especially for high-intensity rainfall  
423 events. In other words, fire aerosols have substantial impacts on the nocturnal  
424 convections, which are associated with the local anticyclonic circulation in the western  
425 Borneo. This effect on nocturnal convections in the western Borneo by fire aerosols will  
426 be discussed further in the next section.

### 427 **3.4 The impact of biomass burning activities on nocturnal** 428 **convections in the Borneo region**

429 To further analyze the effects of fire aerosols on nocturnal convections, we have  
430 categorized convective events into nocturnal convections (NC) and non-nocturnal  
431 convections (non-NC), based on whether the maximum rainfall occurs from midnight to  
432 early morning or in the time frame from late afternoon to evening. Figure 10 shows the  
433 diurnal time series of precipitation averaged over the Borneo region ( $r_2$ ) in FF and FFBB.



434 Again, 3-hour-mean rainfalls of nocturnal convections are higher than those of non-  
435 nocturnal convections in both simulations.

436 Nocturnal convections tend to stay close to the west coast associated with a lower-  
437 level convergence enhanced by the prevailing wind and local circulations mainly related  
438 to the land breezes from inland of the western Borneo. The strong convergence near the  
439 surface over the offshore region of the west coast causes the weak westerly monsoon  
440 windflaws and local land breezes to merge during the nighttime. However, during the  
441 fire periods, the daytime absorption of fire aerosols (e.g., black carbon) can cause an  
442 atmospheric warming (even without fire generated heating flux being incorporated in the  
443 model). This could increase near surface air temperature, weaken land breezes and thus  
444 surface convergence. As a result, the nocturnal convections in FFBB cannot develop as  
445 strong as those in FF. On the other hand, both nocturnal and non-nocturnal convections  
446 are initiated over the western mountain range under a prevailing wind of the sea breezes  
447 from the South China Sea. The increases of near surface temperature owing to the fire  
448 aerosols can enhance this prevailing wind from the ocean and thus lead to a higher  
449 convective rainfall in FFBB during the onset stage of the nocturnal convections as well as  
450 non-nocturnal convections.

451 Diurnal evolution of vertical profiles clearly indicates that mass mixing ratio of total  
452 hydrometeors, temperature, and vertical velocity differ in both daytime and nighttime  
453 between FF and FFBB for those nocturnal convections (Fig. 11). The differences of near  
454 surface temperature between FF and FFBB are more pronounced during the period after  
455 sunset (Fig. 11d). The differences of near surface temperature mainly happen over land,



456 and the higher near surface temperature in FFBB weakens the land breezes and near  
457 surface convergence along the coast. Starting from late afternoon, (about 5 PM local  
458 time), vertical velocity increases with time until sunrise next day in both simulations (Fig.  
459 11e) due to the convergence of the monsoon windflaws and local land breezes during the  
460 nighttime, and this matches very well with that of mass mixing ratio of total  
461 hydrometeors (Fig. 11a and 11e). Noticeably, the main differences in vertical velocity  
462 and hydrometeor mass mixing ratio between FFBB and FF also start to become evident  
463 after entering the evening. Because of the weaker convergence near the surface in FFBB,  
464 the differences in vertical velocity at the higher altitude between FFBB and FF peaks in  
465 the nighttime.

466 It should be indicated that if the heat flux generated by fires was incorporated in the  
467 model, the warming effects from biomass burning would be even stronger and could  
468 persist in nocturnal timeframe as demonstrated in Zhang et al. (2019). However, this  
469 would likely be more effective for open fire regime. For most of peat fires, burning is  
470 largely proceeded underground. Based on our significantly reduced heat flux for the peat  
471 fires as discussed in Sect. 2.1, if the heat flux was incorporated in the model, such fires  
472 would not increase surface temperature by 4-5 °C as suggested for the tropical (open) fire  
473 cases in Zhang et al. (2019).

474 As a summary, the schematics shown in Fig. 12 illustrate the impact of biomass  
475 burning activities on nocturnal convections in the Borneo region. In the daytime, under  
476 the prevailing wind of sea breezes from the South China Sea, convections develop over  
477 the western mountain range. Because near surface heating from the absorption of



478 sunlight by fire aerosols could enhance the prevailing wind from the ocean, convective  
479 rainfall becomes higher at the onset stage of the nocturnal convections (still in daytime)  
480 due to biomass burning activities (Fig. 12b). In the nighttime, convection moves to the  
481 offshore region of the western Borneo. The strong convergences near the surface merge  
482 the weak westerly monsoon windflaws with local nighttime land breezes to form an  
483 anticyclonic circulation (Fig. 12c). During the fire periods, the daytime near surface  
484 warming by fire aerosols could also further weaken land breezes and surface  
485 convergence. Hence, the nocturnal convections during fire events would not develop as  
486 strong as in days without fires (Fig. 12d versus 12c).

#### 487 **4 Summary**

488 By comparing WRF-Chem modeling results include or exclude biomass burning  
489 emissions (FFBB versus FF), we have identified certain detailed impacts of fire aerosols  
490 on convective events within two study regions in the Maritime Continent during a four-  
491 month period (June 2008 ~ September 2008). In total, 54 convective systems in the  
492 Sumatra region and 35 convective systems in the Borneo region have been simulated.  
493 Three convective events of each study region have been selected for in-depth  
494 investigation. In addition, statistical analyses have been performed throughout the entire  
495 simulation period for each region. We have focused our analyses on two rainfall  
496 features: 1) convective precipitation associated with Sumatra squall lines, and 2) diurnal  
497 rainfall over the western Borneo.

498 We find that fire aerosols lead to the increase of cloud water mass and cloud droplet  
499 number concentration among all analyzed cases while a substantial reduction of rain drop  
500 number concentration. Influences of fire aerosols on other hydrometeors vary from case



501 to case. Specifically, our results show that fire aerosols can significantly change the  
502 quantities of hydrometeors, particularly those involved in cold cloud processes and  
503 rainfall of weak convections in either the Sumatra region or the Borneo region. Rainfall  
504 intensity is higher in FFBB during the entire convection life cycle in those weak  
505 convection cases, and the nighttime rainfall intensity in FFBB is significantly higher than  
506 that in FF.

507 Statistics performed throughout the entire modeled fire season shows that the fire  
508 aerosols only cause a nearly negligible change (2-3%) to the total rainfall of convective  
509 systems in both study regions. On the other hand, we notice that fire aerosols can still  
510 alter daily maximum and minimum rainfall in some cases, for example, fire aerosols lead  
511 to the increase of maximum and minimum rainfall intensity in 30 weak convective events  
512 in the Sumatra region.

513 In the Borneo region, biomass burning activities mainly affect the rainfall intensity  
514 of nocturnal convection. Because near surface heating from the absorption of fire  
515 aerosols can enhance the prevailing wind from the ocean (sea breeze) during the daytime,  
516 the convective rainfall over the western mountain range is higher during the onset stage  
517 of the nocturnal convections. In the nighttime, the consequence of the above  
518 thermodynamic perturbation by absorbing fire aerosols can further weaken land breeze  
519 and surface convergence. Hence, the rainfall intensity of nocturnal convections under the  
520 influence of fire aerosols would become weaker.

521 This study has demonstrated how biomass burning activities could affect convective  
522 systems in the Maritime Continent by altering cloud microphysics and dynamics. We  
523 find the biomass burning activities significantly change the diurnal rainfall intensity,



524 especially those low-level wind patterns associated with the weak westerly (WW) regime  
525 as suggested by Ichikawa and Yasunari (2006). Our results show that neither a single  
526 case study nor a simple statistical summary applied to overall model simulation period  
527 without in-depth analyses could reveal the impact of biomass burning aerosols on  
528 convections under different windflow regimes.

### 529 **Data availability**

530 FINNv1.5 emission data are publicly available from  
531 <http://bai.acom.uar.edu/Data/fire/>. REAS emission data can be downloaded from  
532 <https://www.nies.go.jp/REAS/>. TRMM data can be obtained from  
533 <https://pmm.nasa.gov/data-access/downloads/trmm>. AOD from MODIS can be  
534 obtained from [http://dx.doi.org/10.5067/MODIS/MOD08\\_M3.061](http://dx.doi.org/10.5067/MODIS/MOD08_M3.061). Sounding profiles  
535 are publicly available on <http://weather.uwyo.edu/upperair/sounding.html>. WRF-Chem  
536 simulated data are available upon request from Hsiang-He Lee ([lee1061@llnl.gov](mailto:lee1061@llnl.gov)).

### 537 **Author contribution**

538 H.-H. L. and C. W. designed the experiments and H.-H. L. carried them out. H.-H.  
539 L. configured the simulations and analyzed the results. H.-H. L. and C. W. wrote the  
540 manuscript.

### 541 **Acknowledgments**

542 This research was supported by the National Research Foundation Singapore through  
543 the Singapore-MIT Alliance for Research and Technology, the interdisciplinary research



544 program of Center for Environmental Sensing and Modeling. It was also supported by  
545 the U.S. National Science Foundation (AGS-1339264) and L'Agence National de la  
546 Recherche (ANR) of France through the Make-Our-Planet-Great-Again Initiative, ANR-  
547 18-MPGA-003 EUROACE. The authors would like to acknowledge NCEP-FNL and  
548 NCAR FINN working groups for releasing their data to the research communities; and  
549 the NCAR WRF developing team for providing the numerical model for this study. The  
550 computational work for this article was performed on resources of the National  
551 Supercomputing Centre, Singapore (<https://www.nscg.sg>).

552

553

554

555

556



## 557 Reference:

- 558 Ackermann, I. J., Hass, H., Memmesheimer, M., Ebel, A., Binkowski, F. S., and Shankar,  
559 U.: Modal aerosol dynamics model for Europe: development and first  
560 applications, *Atmospheric Environment*, 32, 2981-2999,  
561 [http://dx.doi.org/10.1016/S1352-2310\(98\)00006-5](http://dx.doi.org/10.1016/S1352-2310(98)00006-5), 1998.
- 562 Andreae, M. O., and Gelencsér, A.: Black carbon or brown carbon? The nature of  
563 light-absorbing carbonaceous aerosols, *Atmos. Chem. Phys.*, 6, 3131-3148,  
564 10.5194/acp-6-3131-2006, 2006.
- 565 Chang, C.-P., Millard, J. E., and Chen, G. T. J.: Gravitational Character of Cold Surges  
566 during Winter MONEX, *Monthly Weather Review*, 111, 293-307, 10.1175/1520-  
567 0493(1983)111<0293:gcoocsd>2.0.co;2, 1983.
- 568 Chang, C.-P., Harr, P. A., and Chen, H.-J.: Synoptic Disturbances over the Equatorial  
569 South China Sea and Western Maritime Continent during Boreal Winter,  
570 *Monthly Weather Review*, 133, 489-503, 10.1175/mwr-2868.1, 2005.
- 571 Crippa, P., Castruccio, S., Archer-Nicholls, S., Lebron, G. B., Kuwata, M., Thota, A.,  
572 Sumin, S., Butt, E., Wiedinmyer, C., and Spracklen, D. V.: Population exposure to  
573 hazardous air quality due to the 2015 fires in Equatorial Asia, *Scientific Reports*,  
574 6, 37074, 10.1038/srep37074, 2016.
- 575 Frankenberg, E., McKee, D., and Thomas, D.: Health consequences of forest fires in  
576 Indonesia, *Demography*, 42, 109-129, 10.1353/dem.2005.0004, 2005.
- 577 Freitas, S. R., Longo, K. M., Chatfield, R., Latham, D., Silva Dias, M. A. F., Andreae, M. O.,  
578 Prins, E., Santos, J. C., Gielow, R., and Carvalho Jr, J. A.: Including the sub-grid  
579 scale plume rise of vegetation fires in low resolution atmospheric transport  
580 models, *Atmos. Chem. Phys.*, 7, 3385-3398, 10.5194/acp-7-3385-2007, 2007.
- 581 Fujii, Y., Iriana, W., Oda, M., Puriwigati, A., Tohno, S., Lestari, P., Mizohata, A., and  
582 Huboyo, H. S.: Characteristics of carbonaceous aerosols emitted from peatland  
583 fire in Riau, Sumatra, Indonesia, *Atmospheric Environment*, 87, 164-169,  
584 <http://dx.doi.org/10.1016/j.atmosenv.2014.01.037>, 2014.
- 585 Ge, C., Wang, J., and Reid, J. S.: Mesoscale modeling of smoke transport over the  
586 Southeast Asian Maritime Continent: coupling of smoke direct radiative effect  
587 below and above the low-level clouds, *Atmos. Chem. Phys.*, 14, 159-174,  
588 10.5194/acp-14-159-2014, 2014.
- 589 Grandey, B. S., Lee, H. H., and Wang, C.: Radiative effects of interannually varying vs.  
590 interannually invariant aerosol emissions from fires, *Atmos. Chem. Phys.*, 16,  
591 14495-14513, 10.5194/acp-16-14495-2016, 2016.
- 592 Grell, G. A., Peckham, S. E., Schmitz, R., McKeen, S. A., Frost, G., Skamarock, W. C., and  
593 Eder, B.: Fully coupled "online" chemistry within the WRF model, *Atmospheric  
594 Environment*, 39, 6957-6975, 10.1016/j.atmosenv.2005.04.027, 2005.
- 595 Grell, G. A., and Freitas, S. R.: A scale and aerosol aware stochastic convective  
596 parameterization for weather and air quality modeling, *Atmos. Chem. Phys.*, 14,  
597 5233-5250, 10.5194/acp-14-5233-2014, 2014.
- 598 Hodzic, A., and Duvel, J. P.: Impact of Biomass Burning Aerosols on the Diurnal Cycle  
599 of Convective Clouds and Precipitation Over a Tropical Island, *Journal of*



- 600 Geophysical Research: Atmospheres, 123, 1017-1036, 10.1002/2017JD027521,  
601 2017.
- 602 Huffman, G. J., Bolvin, D. T., Nelkin, E. J., Wolff, D. B., Adler, R. F., Gu, G., Hong, Y.,  
603 Bowman, K. P., and Stocker, E. F.: The TRMM Multisatellite Precipitation  
604 Analysis (TMPA): Quasi-Global, Multiyear, Combined-Sensor Precipitation  
605 Estimates at Fine Scales, *Journal of Hydrometeorology*, 8, 38-55,  
606 10.1175/JHM560.1, 2007.
- 607 Iacono, M. J., Delamere, J. S., Mlawer, E. J., Shephard, M. W., Clough, S. A., and Collins,  
608 W. D.: Radiative forcing by long-lived greenhouse gases: Calculations with the  
609 AER radiative transfer models, *Journal of Geophysical Research: Atmospheres*,  
610 113, 10.1029/2008JD009944, 2008.
- 611 Ichikawa, H., and Yasunari, T.: Time-Space Characteristics of Diurnal Rainfall over  
612 Borneo and Surrounding Oceans as Observed by TRMM-PR, *Journal of Climate*,  
613 19, 1238-1260, 10.1175/jcli3714.1, 2006.
- 614 Jeong, G. R., and Wang, C.: Climate effects of seasonally varying Biomass Burning  
615 emitted Carbonaceous Aerosols (BBCA), *Atmos. Chem. Phys.*, 10, 8373-8389,  
616 10.5194/acp-10-8373-2010, 2010.
- 617 Koh, T.-Y., and Teo, C.-K.: TOWARD A MESOSCALE OBSERVATION NETWORK IN  
618 SOUTHEAST ASIA, *Bulletin of the American Meteorological Society*, 90, 481-  
619 488, 10.1175/2008bams2561.1, 2009.
- 620 Kunii, O., Kanagawa, S., Yajima, I., Hisamatsu, Y., Yamamura, S., Amagai, T., and  
621 Ismail, I. T. S.: The 1997 Haze Disaster in Indonesia: Its Air Quality and Health  
622 Effects, *Archives of Environmental Health: An International Journal*, 57, 16-22,  
623 10.1080/00039890209602912, 2002.
- 624 Kurokawa, J., Ohara, T., Morikawa, T., Hanayama, S., Janssens-Maenhout, G., Fukui, T.,  
625 Kawashima, K., and Akimoto, H.: Emissions of air pollutants and greenhouse  
626 gases over Asian regions during 2000–2008: Regional Emission inventory in  
627 ASia (REAS) version 2, *Atmos. Chem. Phys.*, 13, 11019-11058, 10.5194/acp-13-  
628 11019-2013, 2013.
- 629 Lee, H.-H., Bar-Or, R. Z., and Wang, C.: Biomass burning aerosols and the low-  
630 visibility events in Southeast Asia, *Atmos. Chem. Phys.*, 17, 965-980,  
631 10.5194/acp-17-965-2017, 2017.
- 632 Lee, H.-H., Iraqui, O., Gu, Y., Yim, S. H. L., Chulakadabba, A., Tonks, A. Y. M., Yang, Z.,  
633 and Wang, C.: Impacts of air pollutants from fire and non-fire emissions on the  
634 regional air quality in Southeast Asia, *Atmos. Chem. Phys.*, 18, 6141-6156,  
635 10.5194/acp-18-6141-2018, 2018.
- 636 Lee, H.-H., Iraqui, O., and Wang, C.: The Impact of Future Fuel Consumption on  
637 Regional Air Quality in Southeast Asia, *Scientific Reports*, 9, 2648,  
638 10.1038/s41598-019-39131-3, 2019.
- 639 Lin, N.-H., Tsay, S.-C., Maring, H. B., Yen, M.-C., Sheu, G.-R., Wang, S.-H., Chi, K. H.,  
640 Chuang, M.-T., Ou-Yang, C.-F., Fu, J. S., Reid, J. S., Lee, C.-T., Wang, L.-C., Wang, J.-  
641 L., Hsu, C. N., Sayer, A. M., Holben, B. N., Chu, Y.-C., Nguyen, X. A., Sopajaree, K.,  
642 Chen, S.-J., Cheng, M.-T., Tsuang, B.-J., Tsai, C.-J., Peng, C.-M., Schnell, R. C.,  
643 Conway, T., Chang, C.-T., Lin, K.-S., Tsai, Y. I., Lee, W.-J., Chang, S.-C., Liu, J.-J.,  
644 Chiang, W.-L., Huang, S.-J., Lin, T.-H., and Liu, G.-R.: An overview of regional  
645 experiments on biomass burning aerosols and related pollutants in Southeast



- 646 Asia: From BASE-ASIA and the Dongsha Experiment to 7-SEAS, Atmospheric  
647 Environment, 78, 1-19, <http://dx.doi.org/10.1016/j.atmosenv.2013.04.066>,  
648 2013.
- 649 Lo, J. C. F., and Orton, T.: The general features of tropical Sumatra Squalls, Weather,  
650 71, 175-178, 10.1002/wea.2748, 2016.
- 651 Miettinen, J., Shi, C., and Liew, S. C.: Deforestation rates in insular Southeast Asia  
652 between 2000 and 2010, Global Change Biology, 17, 2261-2270,  
653 10.1111/j.1365-2486.2011.02398.x, 2011.
- 654 Mlawer, E. J., Taubman, S. J., Brown, P. D., Iacono, M. J., and Clough, S. A.: Radiative  
655 transfer for inhomogeneous atmospheres: RRTM, a validated correlated-k  
656 model for the longwave, Journal of Geophysical Research: Atmospheres, 102,  
657 16663-16682, 10.1029/97JD00237, 1997.
- 658 Morrison, H., Curry, J. A., and Khvorostyanov, V. I.: A New Double-Moment  
659 Microphysics Parameterization for Application in Cloud and Climate Models.  
660 Part I: Description, Journal of the Atmospheric Sciences, 62, 1665-1677,  
661 10.1175/jas3446.1, 2005.
- 662 Morrison, H., Thompson, G., and Tatarskii, V.: Impact of Cloud Microphysics on the  
663 Development of Trailing Stratiform Precipitation in a Simulated Squall Line:  
664 Comparison of One- and Two-Moment Schemes, Monthly Weather Review, 137,  
665 991-1007, 10.1175/2008mwr2556.1, 2009.
- 666 Nakanishi, M., and Niino, H.: Development of an Improved Turbulence Closure  
667 Model for the Atmospheric Boundary Layer, Journal of the Meteorological  
668 Society of Japan. Ser. II, 87, 895-912, 10.2151/jmsj.87.895, 2009.
- 669 National Centers for Environmental Prediction, N. W. S. N. U. S. D. o. C.: NCEP FNL  
670 Operational Model Global Tropospheric Analyses, continuing from July 1999,  
671 10.5065/D6M043C6, 2000.
- 672 Oki, T., and Musiak, K.: Seasonal Change of the Diurnal Cycle of Precipitation over  
673 Japan and Malaysia, Journal of Applied Meteorology, 33, 1445-1463,  
674 10.1175/1520-0450(1994)033<1445:scotdc>2.0.co;2, 1994.
- 675 Ramanathan, V., Crutzen, P. J., Lelieveld, J., Mitra, A. P., Althausen, D., Anderson, J.,  
676 Andreae, M. O., Cantrell, W., Cass, G. R., Chung, C. E., Clarke, A. D., Coakley, J. A.,  
677 Collins, W. D., Conant, W. C., Dulac, F., Heintzenberg, J., Heymsfield, A. J., Holben,  
678 B., Howell, S., Hudson, J., Jayaraman, A., Kiehl, J. T., Krishnamurti, T. N., Lubin, D.,  
679 McFarquhar, G., Novakov, T., Ogren, J. A., Podgorny, I. A., Prather, K., Priestley, K.,  
680 Prospero, J. M., Quinn, P. K., Rajeev, K., Rasch, P., Rupert, S., Sadourny, R.,  
681 Satheesh, S. K., Shaw, G. E., Sheridan, P., and Valero, F. P. J.: Indian Ocean  
682 Experiment: An integrated analysis of the climate forcing and effects of the  
683 great Indo-Asian haze, Journal of Geophysical Research: Atmospheres, 106,  
684 28371-28398, 10.1029/2001jd900133, 2001.
- 685 Ramanathan, V., and Carmichael, G.: Global and regional climate changes due to  
686 black carbon, Nature Geosci, 1, 221-227, 2008.
- 687 Rosenfeld, D.: TRMM observed first direct evidence of smoke from forest fires  
688 inhibiting rainfall, Geophysical Research Letters, 26, 3105-3108,  
689 10.1029/1999gl006066, 1999.



- 690 Satheesh, S. K., and Ramanathan, V.: Large differences in tropical aerosol forcing at  
691 the top of the atmosphere and Earth's surface, *Nature*, 405, 60-63,  
692 10.1038/35011039, 2000.
- 693 Schell, B., Ackermann, I. J., Hass, H., Binkowski, F. S., and Ebel, A.: Modeling the  
694 formation of secondary organic aerosol within a comprehensive air quality  
695 model system, *Journal of Geophysical Research: Atmospheres* (1984–2012),  
696 106, 28275-28293, 2001.
- 697 Sekiguchi, M., Nakajima, T., Suzuki, K., Kawamoto, K., Higurashi, A., Rosenfeld, D.,  
698 Sano, I., and Mukai, S.: A study of the direct and indirect effects of aerosols using  
699 global satellite data sets of aerosol and cloud parameters, *Journal of*  
700 *Geophysical Research: Atmospheres*, 108, 4699, 10.1029/2002JD003359, 2003.
- 701 Stockwell, W. R., Kirchner, F., Kuhn, M., and Seefeld, S.: A new mechanism for  
702 regional atmospheric chemistry modeling, *Journal of Geophysical Research:*  
703 *Atmospheres*, 102, 25847-25879, 10.1029/97JD00849, 1997.
- 704 Taylor, D.: Biomass burning, humans and climate change in Southeast Asia,  
705 *Biodivers Conserv*, 19, 1025-1042, 10.1007/s10531-009-9756-6, 2010.
- 706 Tewari, M., F. Chen, W. Wang, J. Dudhia, M. A. LeMone, K. Mitchell, M. Ek, G. Gayno, J.  
707 Wegiel, and Cuenca, R. H.: Implementation and verification of the unified NOAA  
708 land surface model in the WRF model, 20th conference on weather analysis and  
709 forecasting/16th conference on numerical weather prediction, Seattle, WA,  
710 U.S.A., 2004.
- 711 Tosca, M. G., Randerson, J. T., and Zender, C. S.: Global impact of smoke aerosols from  
712 landscape fires on climate and the Hadley circulation, *Atmos. Chem. Phys.*, 13,  
713 5227-5241, 10.5194/acp-13-5227-2013, 2013.
- 714 Wang, C.: A modeling study on the climate impacts of black carbon aerosols, *Journal*  
715 *of Geophysical Research: Atmospheres*, 109, n/a-n/a, 10.1029/2003JD004084,  
716 2004.
- 717 Wang, C.: A modeling study of the response of tropical deep convection to the  
718 increase of cloud condensation nuclei concentration: 1. Dynamics and  
719 microphysics, *Journal of Geophysical Research: Atmospheres*, 110, D21211,  
720 10.1029/2004JD005720, 2005.
- 721 Wiedinmyer, C., Akagi, S. K., Yokelson, R. J., Emmons, L. K., Al-Saadi, J. A., Orlando, J. J.,  
722 and Soja, A. J.: The Fire INventory from NCAR (FINN): a high resolution global  
723 model to estimate the emissions from open burning, *Geosci. Model Dev.*, 4, 625-  
724 641, 10.5194/gmd-4-625-2011, 2011.
- 725 Wu, P., Hara, M., Hamada, J.-i., Yamanaka, M. D., and Kimura, F.: Why a Large Amount  
726 of Rain Falls over the Sea in the Vicinity of Western Sumatra Island during  
727 Nighttime, *Journal of Applied Meteorology and Climatology*, 48, 1345-1361,  
728 10.1175/2009jamc2052.1, 2009.
- 729 Wu, R., Wen, Z., and He, Z.: ENSO Contribution to Aerosol Variations over the  
730 Maritime Continent and the Western North Pacific during 2000–10, *Journal of*  
731 *Climate*, 26, 6541-6560, 10.1175/JCLI-D-12-00253.1, 2013.
- 732 Yi, L., and Lim, H.: Semi-Idealized COAMPS® Simulations of Sumatra Squall Lines:  
733 the Role of Boundary Forcing, in: *Advances in Geosciences*, 111-124, 2006.



734 Zhang, Y., Fan, J., Logan, T., Li, Z., and Homeyer, C. R.: Wildfire impact on  
735 environmental thermodynamics and severe convective storms, Geophysical  
736 Research Letters, 0, 10.1029/2019gl084534, 2019.

737

738



739 Table 1. The case period of the selected cases in the Sumatra region (r1) and the Borneo  
740 region (r2)

Case name	Case period
r1c1	2008/08/10 0900 UTC ~ 2008/08/11 0300 UTC
r1c2	2008/08/19 0600 UTC ~ 2008/08/20 0000 UTC
r1c3	2008/09/23 0900 UTC ~ 2008/09/24 0000 UTC
r2c1	2008/08/05 0900 UTC ~ 2008/08/06 0300 UTC
r2c2	2008/09/17 0600 UTC ~ 2008/09/17 2100 UTC
r2c3	2008/09/22 0300 UTC ~ 2008/09/23 0000 UTC

741  
742  
743



744

Table 2. The fire periods in the two study regions

The Sumatra region (r1)	The Borneo region (r2)
6/10/2008 ~ 6/20/2008	6/21/2008 ~ 6/27/2008
6/25/2008 ~ 6/28/2008	8/1/2008 ~ 8/8/2008
7/4/2008 ~ 7/7/2008	9/10/2008 ~ 9/30/2008
7/27/2008 ~ 8/20/2008	
9/17/2008 ~ 9/27/2008	

745

746



747 Table 3. The mean differences in percentage of FFBB to FF (i.e.  $(FFBB-FF)/FF \times 100\%$ )  
 748 for each selected case over the main convection area in the Sumatra region (r1) and the  
 749 Borneo region (r2). Qc, Qi, Qr, Qs and Qg represents cloud, ice, rain, snow, and graupel  
 750 mass concentration respectively. Qnc, Qni, Qnr, Qns and Qng means number  
 751 concentration for each hydrometeor.

Case	Qc	Qi	Qr	Qs	Qg	Qnc	Qni	Qnr	Qns	Qng
r1c1	8%	27%	49%	62%	48%	248%	55%	-41%	33%	39%
r1c2	20%	-6%	-15%	-25%	1%	349%	-1%	-45%	-11%	-6%
r1c3	18%	10%	-10%	3%	5%	311%	4%	-50%	11%	-6%
r2c1	27%	1%	-6%	-5%	-4%	703%	3%	-59%	4%	-5%
r2c2	22%	10%	64%	69%	58%	337%	24%	-32%	17%	57%
r3c3	8%	10%	19%	60%	-2%	409%	-5%	-66%	8%	-12%

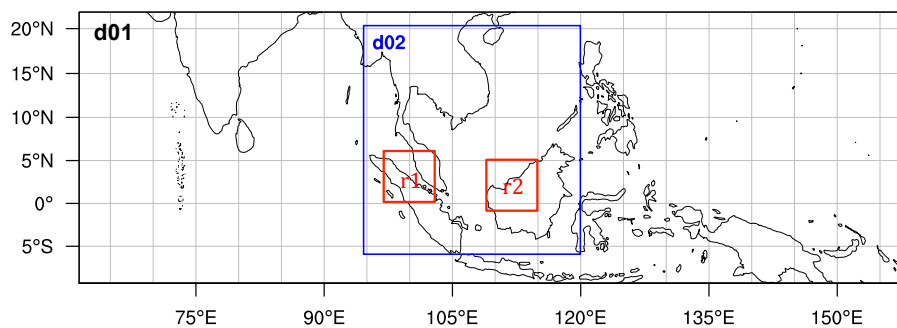
752



753 Table 4. The averaged precipitation ( $\text{mm } 3\text{hrs}^{-1}$ ) of FFBB and FF for each selected case  
754 over the main convection area in the Sumatra region (r1) and the Borneo region (r2).  
755 Parentheses in the third column show the difference in percentage of FFBB to FF (i.e.  
756  $(\text{FFBB}-\text{FF})/\text{FF} \times 100\%$ ).  
757

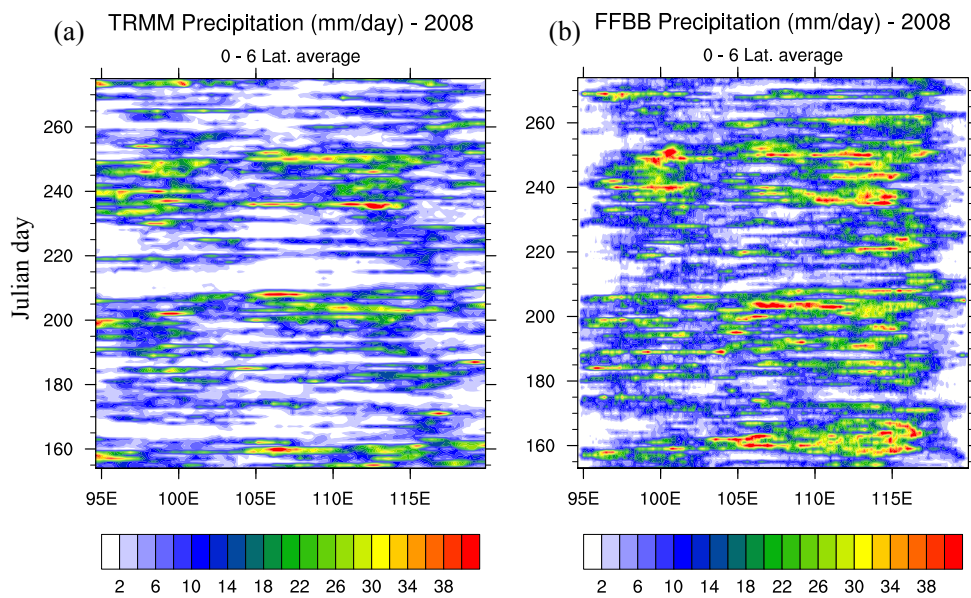
Case	FF	FFBB
r1c1	1.33±0.47	2.74±1.21 (+106%)
r1c2	2.97±1.42	3.05±1.49 (+3%)
r1c3	4.32±1.84	3.98±2.18 (-8%)
r2c1	3.73±2.64	3.07±1.21 (-18%)
r2c2	1.88±0.53	3.97±1.47 (+111%)
r3c3	0.54±0.53	1.10±1.02 (+103%)

758  
759



760  
761  
762  
763  
764  
765  
766

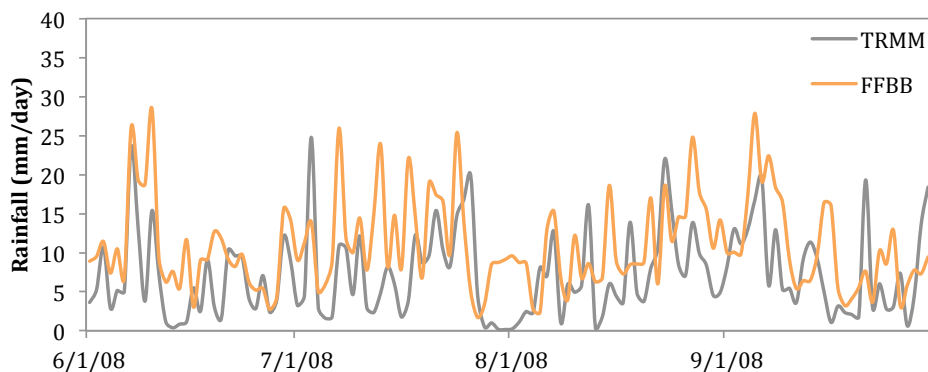
Figure 1. Domain configuration for WRF-Chem simulations. Domain 1 (d01) has a resolution of 25 km, while Domain 2 (d02) has a resolution of 5 km. Two red boxes indicate the two study regions: the Sumatra region (r1) and the Borneo region (r2).



767  
768 Figure 2. Hovmöller (time versus longitude) plot of daily precipitation ( $\text{mm day}^{-1}$ ) from 1  
769 June 2008 to 30 September 2008 from:(a) Tropical Rainfall Measuring Mission (TRMM)  
770 and (b) FFBB. Latitude average is from  $0^\circ$  to  $6^\circ\text{N}$ .  
771

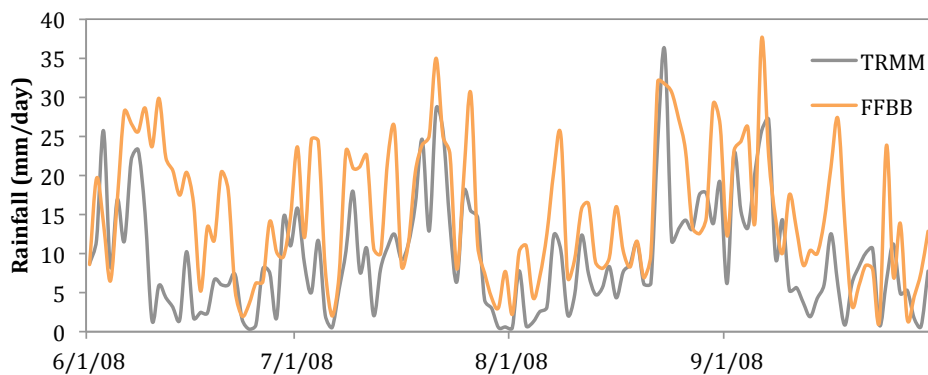


**(a) Rainfall comparison - r1**



772

**(b) Rainfall comparison - r2**



773

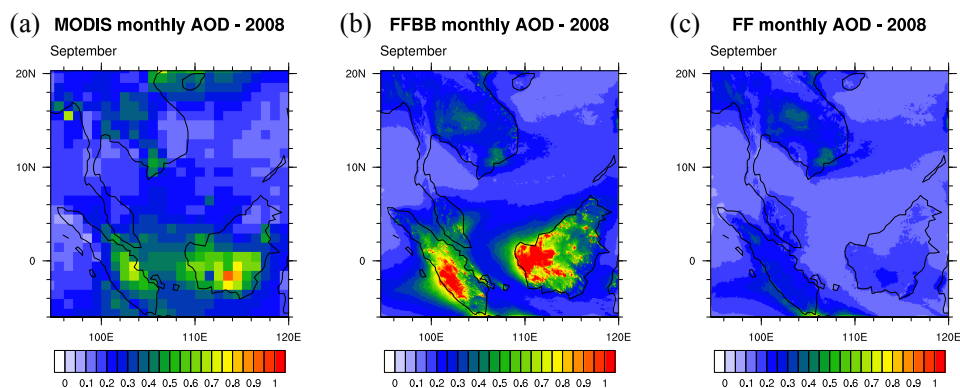
774

775

776

777

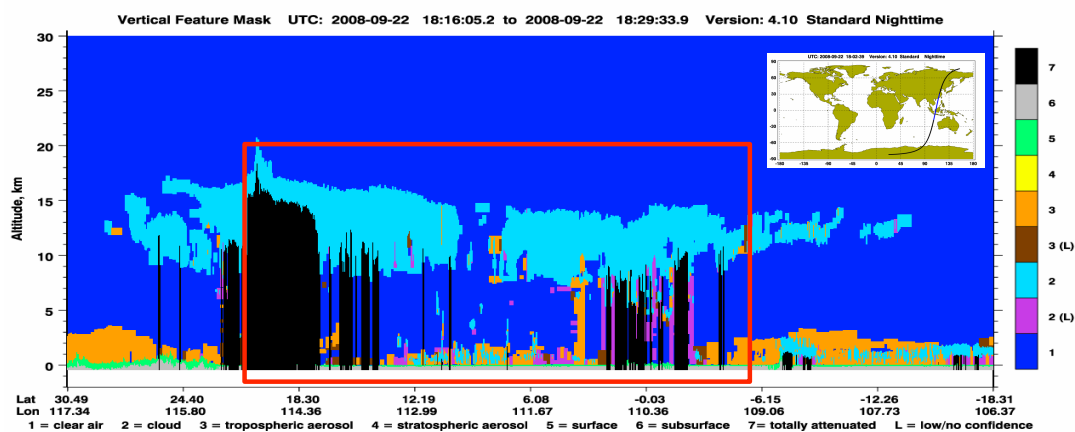
Figure 3. Time series of area-averaged daily rainfall ( $\text{mm day}^{-1}$ ) from Tropical Rainfall Measuring Mission (TRMM) and FFBB over (a) the Sumatra region (r1) and (b) the Borneo region (r2).



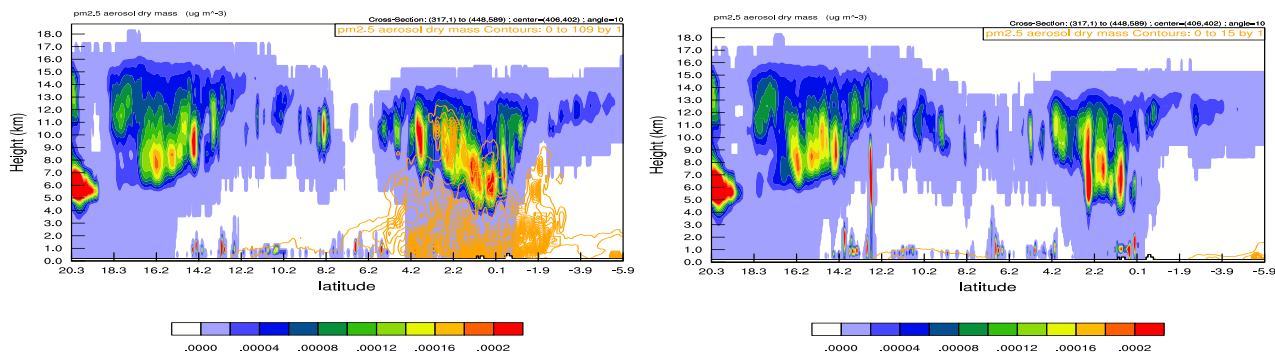
778  
779  
780  
781  
782

Figure 4. Monthly aerosol optical depth (AOD) in September 2008 from (a) Moderate Resolution Imaging Spectroradiometer (MODIS), (b) FFBB, and (c) FF.





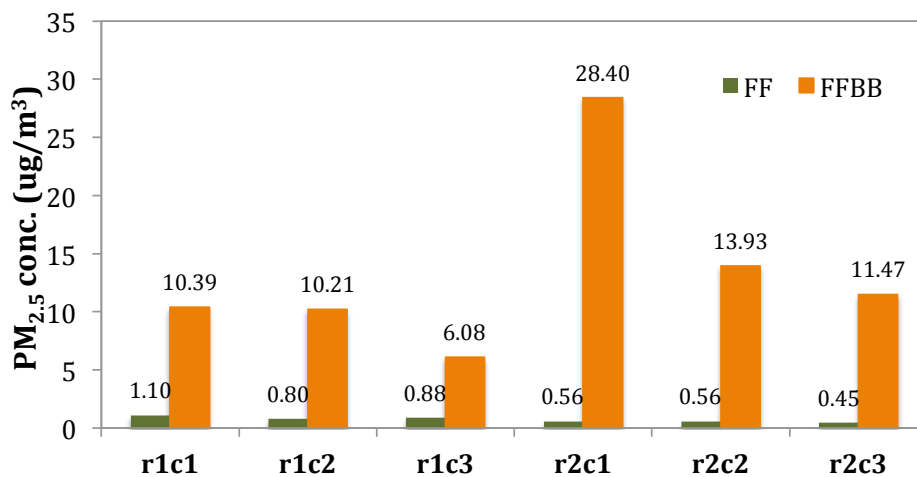
787  
788  
789



790



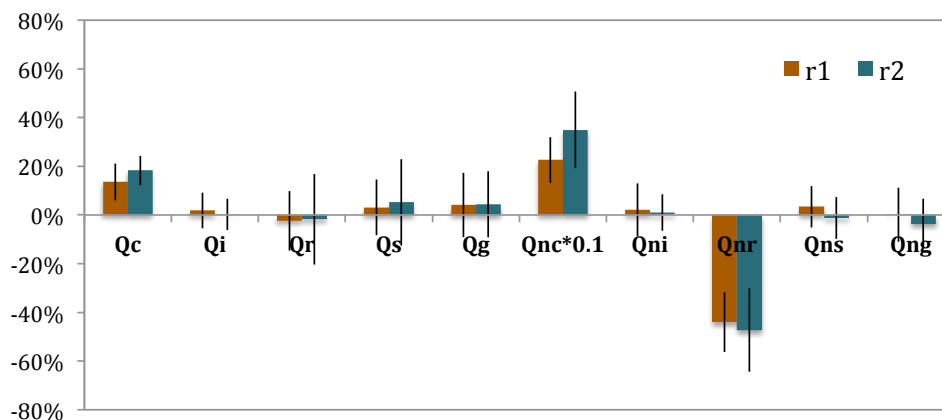
791 Figure 6 (a) The vertical structure of cloud retrieved from the Cloud-Aerosol Lidar and Infrared Pathfinder Satellite Observation  
792 (CALIPSO) on September 22, 2008. (b)-(c) The sum of simulated hydrometeor mixing ratio (shaded;  $\text{kg kg}^{-1}$ ) and  $\text{PM}_{2.5}$  concentration  
793 (contour;  $\mu\text{g m}^{-3}$ ) in FFBB and FF, respectively. The profile domain of (b) and (c) is corresponding to the red rectangle in (a).  
794



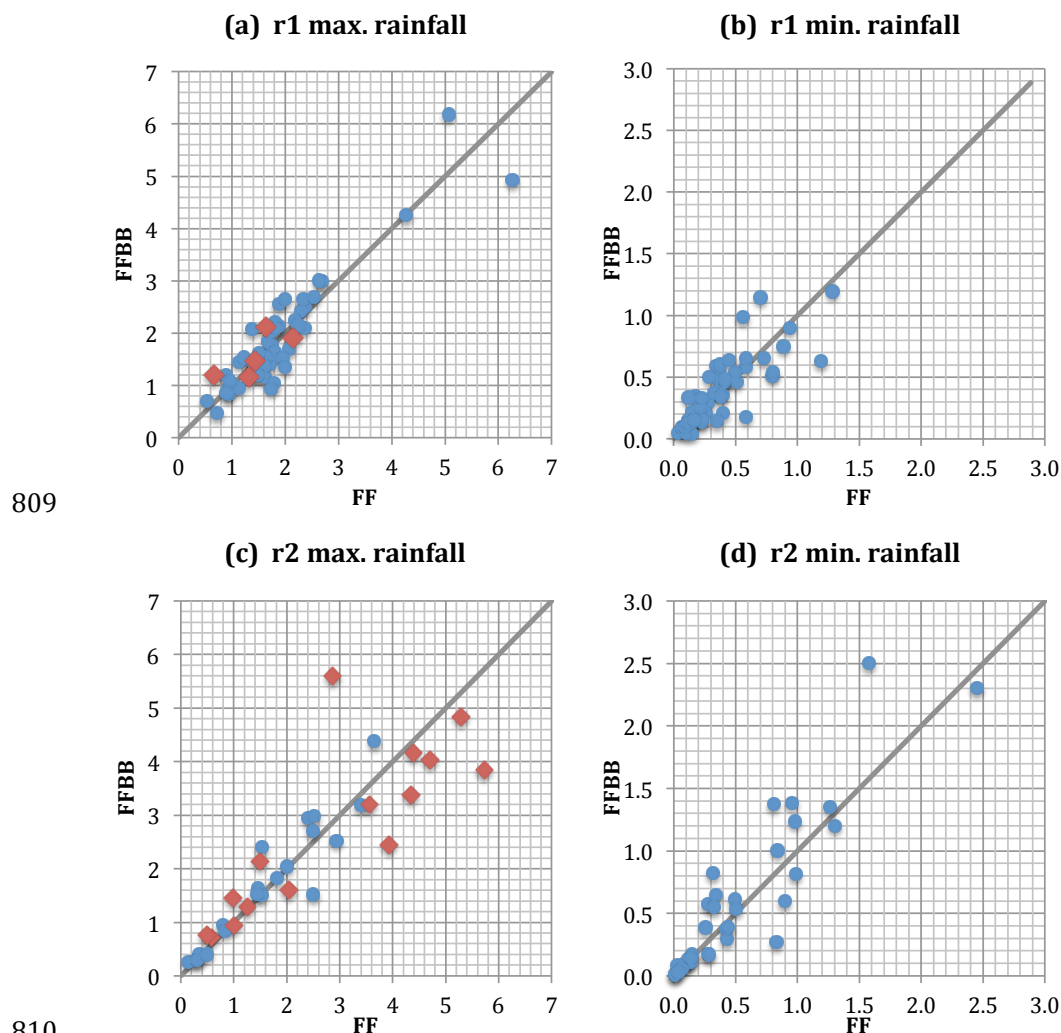
795  
796 Figure 7. The mean PM<sub>2.5</sub> concentration (µg m<sup>-3</sup>) in FF and FFBB for selected cases in the  
797 Sumatra region (r1) and the Borneo region (r2).  
798



799  
800



801  
802 Figure 8. The mean differences in percentage of FFBB to FF (i.e.  $(FFBB-FF)/FF \times 100\%$ )  
803 over all convective cases during the fire periods in the Sumatra region (r1) and the Borneo  
804 region (r2). Qc, Qi, Qr, Qs and Qg represents cloud, ice, rain, snow, and graupel mass  
805 concentration, respectively. Qnc, Qni, Qnr, Qns and Qng means number concentration for  
806 each hydrometeor. The error bars represent one standard deviation.  
807  
808

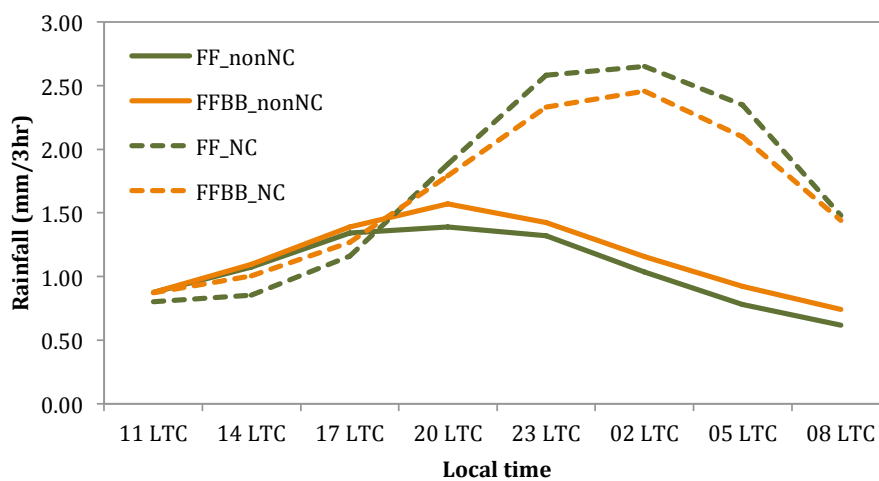


809

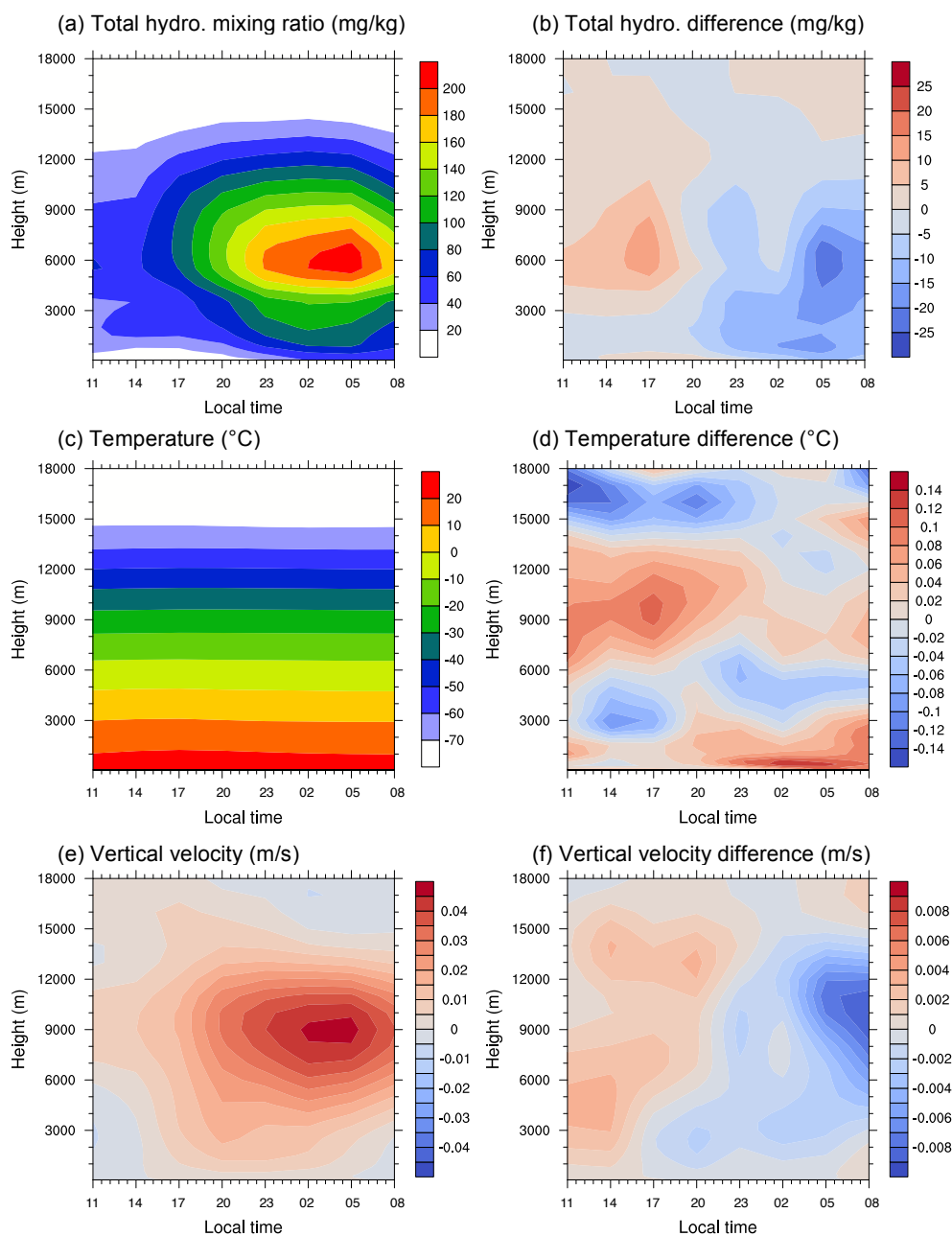
810

811 Figure 9. The scatterplots of daily maximum and minimum convective rainfall ( $\text{mm } 3\text{hr}^{-1}$ )  
812 during the fire periods in in the Sumatra region (r1) and the Borneo region (r2). Red  
813 diamonds in (a) and (c) indicate that the maximum convective rainfall conducts in the  
814 midnight or early morning.

815



816  
817 Figure 10. The diurnal time series of precipitation averaged over the Borneo region ( $r_2$ ) for  
818 nocturnal convections (NC) and non- nocturnal convections (non-NC) during fire periods in  
819 FF and FFBB.  
820  
821



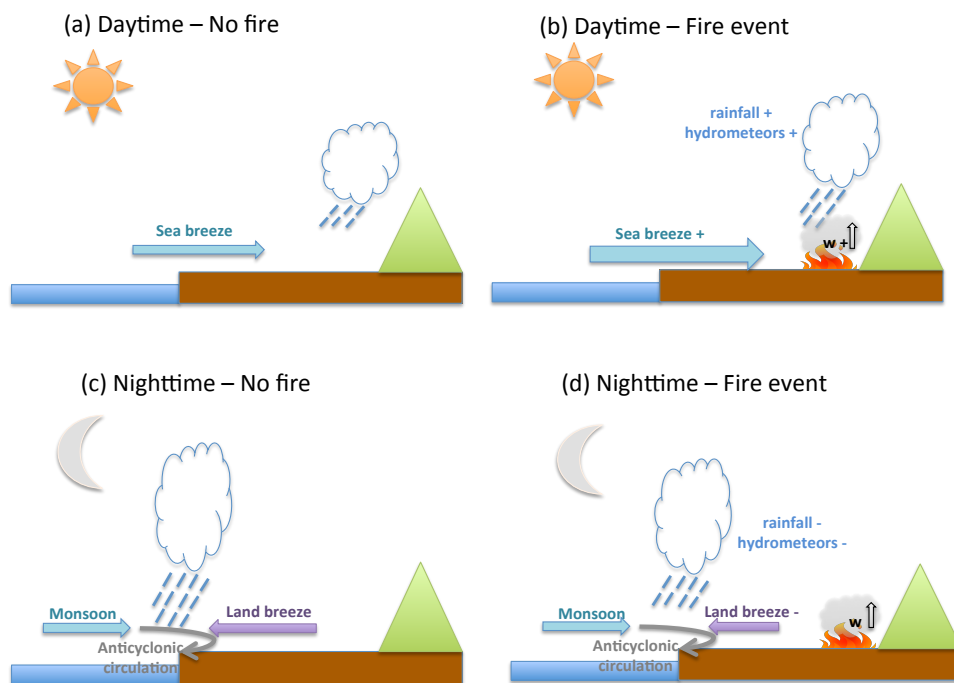
822  
823

824  
825

826

827 Figure 11. Diurnal evolution of vertical profiles over the Borneo region (r2) in FF for (a)  
828 total hydrometeor mixing ratio ( $\text{mg kg}^{-1}$ ), (c) temperature ( $^{\circ}\text{C}$ ), and (e) vertical velocity ( $\text{m s}^{-1}$ ).  
829 Data are averaged all the nocturnal convections. (b), (d), and (f) is the differences  
830 between FF and FFBB (FFBB-FF) for each parameter.

831



832  
833 Figure 12. Schematics of diurnal rainfall/convection activity over the western Borneo. (a)  
834 and (b) illustrate the formation of convection during the daytime without and with fire event,  
835 respectively. (c) and (d) are the same as (a) and (b) but in the nighttime.  
836